https://doi.org/10.1016/j.dyepig.2021.109879

Synthesis and Photophysical Properties of Ternary β-Diketonate Europium(III) Complexes Incorporating Bipyridine and its Derivatives

Idris Juma Al-Busaidi[a], Rashid Ilmi*[a], Danyang Zhang,[b] José D. L. Dutra,[c] Willyan F. Oliveira,[c] Nawal K. Al Rasbi,[a] Liang Zhou,*[b] Wai-Yeung Wong,*[d] Paul R. Raithby,*[e] and Muhammad S. Khan[a]*

[a]Department of Chemistry, Sultan Qaboos University, P. O. Box 36, Al Khod 123, Oman

[b]State Key Laboratory of Rare Earth Resource Utilization, Changchun Institute of Applied Chemistry, Chinese Academy of Sciences, Renmin Street 5625, Changchun 130022, People's Republic of China.

[c]Pople Computational Chemistry Laboratory, Department of Chemistry, UFS, 49100-000 São Cristóvão, Sergipe, Brazil.

[d]Department of Applied Biology and Chemical Technology and Research Institute for Smart Energy, The Hong Kong Polytechnic University, Hung Hom, Kowloon, Hong Kong, People's Republic of China.

[e]Department of Chemistry, University of Bath, Claverton Down, Bath BA2 7AY, UK.

E-mail addresses and ORCID ID of corresponding authors:

Rashid Ilmi : rashidilmi@gmail.com; 0000-0002-5165-5977

Muhammad S. Khan : msk@squ.edu.om; 0000-0001-5606-6832

Liang Zhou : zhoul@ciac.ac.cn; 0000-0002-2751-5974

Wai-Yeung Wong : wai-yeung.wong@polyu.edu.hk; 0000-0002-9949-7525

Paul R. Raithby : p.r.raithby@bath.ac.uk; 0000-0002-2944-0662

Abstract: Two new octa-coordinated ternary europium(III) complexes of the type [Eu(btfa)$_3$(**Br$_2$-bpy**)] (**Eu-1**) and [Eu(btfa)$_3$(**PhE$_2$-bpy**)] (**Eu-2**) (where btfa = 4,4,4-trifluoro-1-phenyl-1,3-butanedione, **Br$_2$-bpy** = 5,5'-dibromo-2,2'-bipyridine, **PhE$_2$-bpy** 5,5'-bis(phenylethynyl)-2,2'-bipyridine) together with a previously reported complex [Eu(btfa)$_3$(**bpy**)] (**Eu-3**) have been synthesized. The complexes have been characterized by analytical and spectroscopic methods. The photophysical properties of the complexes have also been analyzed both experimentally and theoretically. The contribution of each ligand to the sensitized Eu(III) photoluminescence (PL) has been analyzed and is discussed. An energy transfer (ET) mechanism is proposed and discussed for the sensitized Eu(III) emission using experimental and theoretical data. The Eu(III) complex incorporating the parent bpy showed impressive performance as a double-emitting layer (EML) red organic light emitting diodes (R-OLEDs).

Keywords: β-diketone; Photoluminescence; Energy transfer mechanism; Organic light emitting diodes

1. Introduction

The intriguing PL properties of trivalent lanthanide (Ln(III)) complexes make them outstanding candidates for the development of a range of functional materials [1]. However, a frequently encountered bottleneck for Ln(III) ions is the low molar absorptivity due to the forbidden nature of the 4f – 4f electronic transitions, which can be bypassed *via* the "*antenna effect*" [2]. In this strategy, a Ln(III) ion is complexed with organic ligand(s) possessing a strong absorption profile in the ultraviolet (UV) to visible (Vis) region of the spectrum that renders the absorbed energy as the excitation energy for the emitting state of the Ln(III) ion. Moreover, an important parameter to evaluate whether the emission is efficient is the energy gap/difference (ΔE) between the emitting level(s) (for instance ≈ 17,300 cm^{-1} for Eu(III) ion) and ligand lowest triplet state (T_1). A too low as well as a too high ΔE will inevitably lower the efficiency of emission. Consequently, the T_1 state of the ligand should be 2000 cm^{-1} above the metal emitting level for optimum efficiency [3].

Against this backdrop, a range of commercially available antenna ligands along with new ligands have been designed and assessed; these include but are not limited to carboxylates [4], phosphonates [5], picrates [6] etc. [7]. Encompassed by the vast group of organic ligands, β-diketones have served as important antenna ligands and their lanthanide complexes have been extensively studied, especially europium tris(β-diketonates) [8]. However, due to the large size of the Ln(III) ion, the tris(β-diketonate) complexes formed with these metal ions is always accompanied by the solvent molecules in the inner-coordination sphere. The presence of solvent molecules with high-energy oscillators (O−H, N−H, C−H) has a negative effect on the PL properties as they deactivate the excited state of the Ln(III) ion [9]. Nevertheless, this issue can be easily resolved by replacing the solvent molecules by neutral heterocyclic, often bidentate, ancillary ligand(s) (*viz*. N^N, N^O, O^O) that change the overall properties of the resulting complexes and the systems have found applications in a range of modern devices [10]. Out of a large variety of ligands, the bidentate 2,2'-bipyridine (bpy), 1,10-phenanthroline (phen) and its derivatives are among the most studied systems [11]. Thus, in the present work, we have synthesized two new Eu(III) complexes by utilizing asymmetrically fluorinated 4,4,4-trifluoro-1-phenyl-1,3-butanedione (btfa) as the primary antenna ligand that offers many advantages compared to their non-fluorinated counterparts such as increased volatility (an important parameter when fabricating OLEDs), a compatible T_1, reduced non-radiative quenching, etc. To replace the detrimental solvents from the inner-coordination, we have utilized 5,5'-dibromo-2,2'-bipyridine (**Br_2-bpy**) and its acetylide derivative 5,5'-bis(phenylethynyl)-2,2'-bipyridine (**PhE_2-bpy, Scheme 1**) as ancillary ligands to form [Eu(btfa)$_3$(**Br_2-bpy**)] (**Eu-1**, **Chart 1**) and [Eu(btfa)$_3$(**PhE_2-bpy**)] (**Eu-2**, **Chart 1**). The former **Br_2-bpy** ligand could reduce the energy loss and also promote spin–orbit coupling through the heavy-atom effect, which facilitates the intersystem crossing (ISC) [12]. Moreover, the activated bpy could be easily utilized for functionalization

with the additional chromophore. In the present study, we have functionalized the **Br_2-bpy** ancillary ligand by inserting the π electron rich phenylethynyl group that retains its linear structure imparting additional rigidity and conjugation that will improve the absorption profile *via* extending the absorption to visible region and, at the same time, boosting the molar absorption coefficient as noted in our very recent reports [13]. Furthermore, to analyze the effect of substituents on the properties of the **Eu-1** and **Eu-2,** we have also synthesized the known Eu(III) complex incorporating the parent **bpy**, [Eu(btfa)$_3$(**bpy**)] [14] (**Eu-3**, **Chart 1**) which has been used as a benchmark to compare with the two new complexes. The complexes were thoroughly characterized by elemental analysis, mass spectrometry, IR spectroscopy, and thermogravimetric analysis. Detailed experimental and theoretical investigations of the photophysical properties of the complexes have been performed and are discussed, including the radiative (A_R) and non-radiative (A_{NR}) decay rates, radiative lifetime (τ_{rad}), intrinsic quantum yield (Q_{Eu}^{Eu}), energy transfer (ET) mechanism and rates. Finally, **Eu-3** was successfully utilized as an emitter to fabricate single- and double-EMLs red-OLEDs (R-OLEDs).

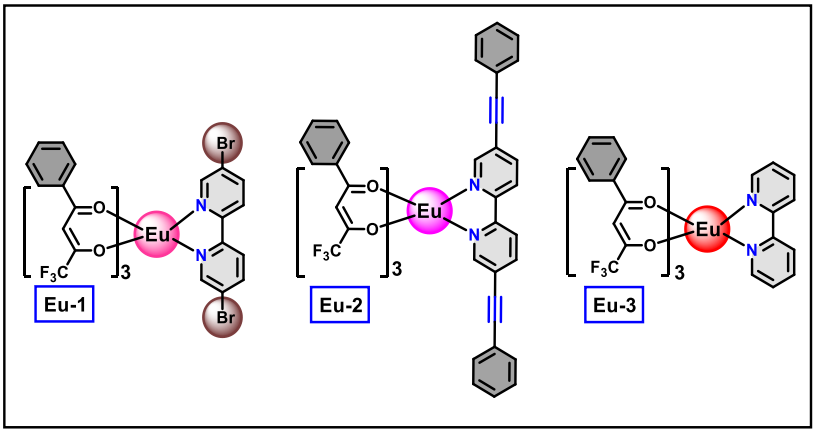

Chart 1. Chemical structures of the mixed-ligand Eu(III) complexes.

2. Experimental

2.1. General

The metal salts $EuCl_3{\cdot}6H_2O$, and $Gd(NO_3)_3{\cdot}6H_2O$ were purchased from Strem Chemicals, Inc. The organic ligands 4,4,4-trifluoro-1-phenyl-1,3-butanedione (Hbtfa), 2,2'-bipyridine (bpy), 5,5'-dibromo-2,2'-bipyridine (**Br_2-bpy,** please see the electronic supporting information [ESI] for the elemental analysis data) were obtained from Tokyo Chemical Industry (TCI) while phenylacetylene was procured from Sigma-Aldrich and used without further purification. Solvents were pre-dried and distilled before use according to standard procedures. Synthesis of the secondary ancillary ligand **PhE_2-bpy** was performed under dry dinitrogen (N_2) atmosphere using standard Schlenk line techniques. The precursor complex [Eu(btfa)$_3$(H_2O)$_2$] was synthesized using literature procedures and characterized by elemental analysis

(data is included in ESI) [15]. Elemental analysis was performed on Euro EA – CHN in the Department of Chemistry, Sultan Qaboos University. Attenuated total-reflectance (ATR) infrared (IR) spectra were recorded on pure samples on diamond using a Cary 630 FT-IR spectrometer. Mass spectra were obtained using LCMS-8040, Shimazdu-Japan coupled to a triple quadruple tandem mass spectrometer equipped with electrospray ionization (**ESI**). All the spectroscopic measurements were performed at room temperature in dichloromethane (DCM:CH_2Cl_2) as the solvent medium. The UV–visible absorption spectra of the ligands and complexes were recorded on a Varian Cary 50 spectrophotometer. Quartz cuvettes of 1 cm path length were used, and solvent background corrections were applied. The fluorescence spectrum of **Br_2-bpy** and **PhE_2-bpy** were recorded on a Shimadzu RF-5301 spectrofluorophotometer. The steady-state emission and excitation spectra of the Eu(III) complexes and their respective phosphorescence lifetimes in solution were recorded on an Edinburgh FS5 fluorimeter. The phosphorescence decay of **Eu-1, Eu-2** and **Eu-3** were monitored at different excitation wavelengths 376, 373 and 406 nm, respectively, using a LED. The measured luminescent decays were fitted to exponential functions convoluted with the system response function. The goodness of the fits was judged by the value of the reduced chi-squared (χ^2).

2.2. Synthesis of ancillary ligand and mixed-ligand ternary europium complexes

2.2.1. Ancillary ligand 5,5'-bis(phenylethynyl)-2,2'-bipyridine (PhE_2-bpy)

To a stirring solution of phenylacetylene (0.50 g, 2.0 mmol) and **Br_2-bpy** (0.77 g, 1.0 mmol) in CH_2Cl_2/^{i}Pr_2NH (50 cm^3, 1:1 v/v) under N_2 was added, a catalytic amount (~5 mg) of CuI and $Pd(OAc)_2$ and Ph_3P. The yellow solution was stirred at room temperature. for 15 h, after which all volatile components were removed under reduced pressure. The residue was redissolved in CH_2Cl_2 and passed through a silica column eluting with hexane/CH_2Cl_2 (1:1, v/v). Removal of the solvents under reduced pressure yielded a yellowish-gold solid (0.43 g, 88%). Calc. for $C_{26}H_{16}N_2$: C, 87.62; H, 4.52; N, 7.86%. Found: C, 87.78; H, 4.47; N, 7.98 %. IR/ cm^{-1} (2215) (-C≡C-) **(Fig. S1, ESI)**. LC-MS: Cal/Obs: 356.13/357.7 [M+H] **(Fig. S2, ESI)**.

2.2.2. [Eu(btfa)$_3$(Br_2-bpy)] (Eu-1)

A solution of **Br_2bpy** (37.43 g, 0.12 mmol) in MeOH/CH_2Cl_2 (10 mL) was added to a solution of [Eu(btfa)$_3$(H_2O)$_2$] (0.1 g, 0.12 mmol) in MeOH/CH_2Cl_2 (10 mL). The reaction mixture was left overnight with stirring at room temperature and was left for the solvent to evaporate slowly yielding a white solid (0.085g). Calc. for $C_{70}H_{45}Br_2EuF_{18}N_2O_{12}$: C, 47.77; H, 2.58; N, 1.59%. Found: C, 47.71; H, 2.49; N, 1.53 %. IR/ cm^{-1} 1608 (C=O), 1561, 1530, 1489, 1451 (C=C, C=O) **(Fig. S3, ESI)**. LC-MS: Cal/Obs: 1109.91/1112 [M+H] **(Fig. S4, ESI)**.

2.2.3. [Eu(btfa)$_3$(PhE$_2$-bpy)] (Eu-2)

A similar synthetic procedure was used to obtain the mixed ligand complex **Eu-2** with **PhE$_2$-bpy** (42.77 g, 0.12 mmol) and [Eu(btfa)$_3$(H$_2$O)$_2$] (0.1 g, 0.12 mmol) in EtOH/CH$_2$Cl$_2$ (10 mL) that yielded a pale-yellow solid (0.075g). Calc. for $C_{56}H_{34}EuF_9N_2O_6$: C, 58.29; H, 2.97; N, 2.43%. Found: C, 58.21; H, 2.92; N, 2.69 %. IR/ cm^{-1} 2214 (-C≡C-), 1606 (C=O), 1572, 1526, 1472, 1461 (C=C, C=N) **(Fig. S5, ESI)**. LC-MS: Cal/Obs: 1154.15/1136.90 [M- H$_2$O+H] **(Fig. S6, ESI)**.

2.2.4. [Eu(btfa)$_3$(bpy)] (Eu-3)

Eu-3 was synthesized by adopting similar synthetic procedure as described above for **Eu-1** and **Eu-2** [**bpy** (18.74 g, 0.12 mmol) and [Eu(btfa)$_3$(H$_2$O)$_2$] (0.1 g, 0.12 mmol) in MeOH/CH$_2$Cl$_2$ (10 mL)], which differs from the previously reported [14] method. The solution was left for slow solvent evaporation, after which pink crystals were obtained (0.090g). Calc. for $C_{40}H_{26}EuF_9N_2O_6$: C, 50.38; H, 2.75; N, 2.94%. Found C, 50.34; H, 2.75; N,2.91%. IR/ cm^{-1} 1608 (C=O), 1572, 1528, 1522, 1487, 1462 (C=C, C=O) **(Fig. S7, ESI)**. LC-MS: Cal/Obs: 954.09 /954 [M+] **(Fig. S8, ESI)**.

To determine the lowest triplet state of the ligands **(Br$_2$-bpy** and **PhE$_2$-bpy)** and to underpin the energy transfer (ET) process, we have also synthesized the Gd(III) complexes of the respective ligands. Their synthesis and characterization (**Fig. S9 – Fig. S12, ESI**) are detailed in the **ESI** (**Section 3**).

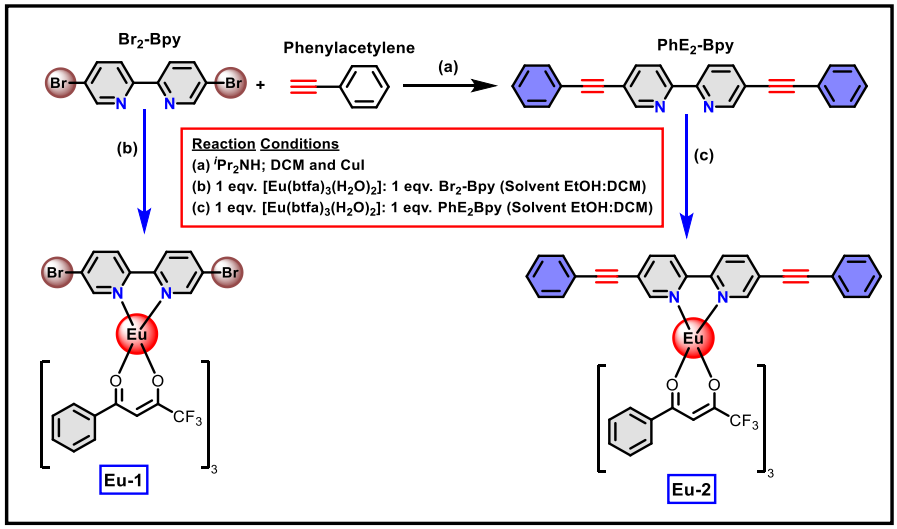

Scheme 1. Synthetic pathways to obtain the ancillary **PhE$_2$-bpy** ligand, and the **Eu-1** and **Eu-2** mixed ligand complexes.

2.3. Theoretical calculations and spectroscopic measurements

Despite repeated attempts, we were not able to grow single crystals of the complexes **Eu-1** and **Eu-2**; however, the structure of the **Eu-3** has been reported previously.[14] Details of the theoretical calculations are elaborated in the **ESI** (**Section 5**). To understand the photophysical phenomenon in a given complex, it is necessary to obtain the theoretical ground state geometry of the complex. We have utilized our own

single-crystal X-ray structure data for **Eu-3** as the input structure to perform the theoretical calculation and for ET studies (Please see the details in **Section 5**, **ESI**). Important photophysical parameters such as the Judd-Ofelt (J-O) intensity parameter (Ω_2 and Ω_4), A_R , A_{NR} decay rates, τ_{rad} , Q_{Eu}^{Eu} of the complexes was estimated with the help of the equations S1 – S7, **ESI** and the details are discussed in our recently reported paper [1d]. The experimental PLQYs (Q_{Eu}^{L}) of Eu(III) complexes were measured by the reported literature method [16] relative to $[Eu(btfa)_3(H_2O)_2]$ [17]. The excitation wavelength was 360 nm and measurements were carried out at room temperature, with a slit width of 1.0 nm for the excitation and for the emission.

2.4. Fabrication of OLEDs and assessments of their EL performance

An ITO coated glass with a sheet resistance of 10 Ω/sq was used as the anode substrate. Prior to the film deposition, patterned ITO substrates were cleaned with detergent, rinsed in de-ionized water, and finally dried in an oven. All organic layers were deposited at a rate of 0.1 nm/s under high vacuum (≤ 3.0×10^{-5} Pa). The doped EMLs were prepared by co-evaporating dopant and host material from two sources, and the doping concentration was modulated by controlling the evaporation rate of the dopant. LiF and Al were deposited in another vacuum chamber (≤ 8.0×10^{-5} Pa) at rates of 0.01 and 1.0 nm/s, respectively, without being exposed to the atmosphere. The thicknesses of these deposited layers and the evaporation rate of individual materials were monitored in vacuum with quartz crystal monitors. A shadow mask was used to define the cathode and make eight emitting dots with an active area of 9 mm^2 on each substrate. Current density (J) – brightness (B) – voltage (V) characteristics were measured by using a programmable brightness light distribution characteristics measurement system C9920-11 from the Hamamatsu Photonic instrument. PL and EL spectra were measured with a calibrated Hitachi F−7000 fluorescence spectrophotometer and an Ocean Optics spectrophotometer.

3. Results and discussion

3.1. Synthesis, Characterization and Determination of the Ground State Geometry

The ancillary ligand **PhE_2-bpy** (**Scheme 1**) was synthesized using a modified Sonogashira method [18] free of palladium(II) and triphenylphosphine by the direct reaction of **Br_2-bpy** with phenylacetylene in 1:1 diisopropylamine ($^{i}Pr_2NH$):CH_2Cl_2 solution using copper(I) iodide (CuI) catalyst. The ligand was thoroughly characterized before complexation. The complexes (**Eu-1, Eu-2** and the known complex **Eu-3)** (**Scheme 1**) were synthesized by reacting the binary hydrated $[Eu(btfa)_3(H_2O)_2]$ complex and the corresponding ancillary ligands (**Br_2-bpy**, **PhE_2-bpy** and **bpy**) in a 1:1 ratio. The formulation of the complexes was established by elemental analysis, FT-IR, and LC-MS. The elemental analyses agree with the proposed formulation for the newly synthesized complexes as shown in **Scheme 1.** The results were further confirmed by the LC-MS spectra of **Eu-1, Eu-2** and **Eu-3** in negative and positive modes

that showed molecular ion peaks at m/z ≈ 1112 [M+H], 1113.8 [M+H], and 954 [M+], respectively for **Eu-1, Eu-2** and **Eu-3 (Figs. S4, S6** and **S8, ESI)**. The FT-IR spectra of the complexes do not display any O-H vibration peaks indicating the coordination of the ancillary ligands to the Eu(III) ion. Moreover, the spectra of the complexes are similar in the region 600 – 1700 cm^{-1} and display C=O, C=C and C=N stretching vibrations typical for these types of complexes[1c, 1d, 10f] due to almost identical skeletons. The **Eu-2** complex shows an absorption peak at 2214 cm^{-1} due to the acetylide group. The ground state geometry of the complexes was determined by different quantum-mechanical methods. Details of the theoretical approaches involved in the elucidation of the geometry and the discussion are included in the ESI (Please see Sections 6.1 and 7.1, **Fig. S13** and **Table S1** – **S3**, ESI).

3.2. Experimental and Theoretical Photophysical Properties of the Complexes

3.2.1. Absorption spectroscopy

Organo-lanthanide complexes that display efficient emitting properties suitable for device applications must meet some of the mandatory requirements such as strong light-absorbing organic ligand(s) that would result in strong light absorbing complexes and an appropriate ΔE between the triplet state of the ligand(s) and the emitting level of the Ln(III) ion [3]. To check the first condition the optical absorption spectra of the bipyridine-based ligands (**Br_2-bpy, PhE_2-bpy** and **bpy**) and their corresponding (**Eu-1**, **Eu-2**, and **Eu-3**) complexes were recorded in CH_2Cl_2 solution (c = 1 x 10^{-5} M) at room temperature as shown in **Fig. 1a** (**Fig. S14**. **ESI)**. The spectra of the free ligands exhibit strong absorptions in the UV region and thus could be utilized to form strong absorbing complexes. Moreover, the spectra of the newly synthesized **PhE_2-bpy** free ligand displays $\lambda_{\max}^{abs}$ = 312 nm and exhibits a redshift of 18 nm and 29 nm compared to **Br_2-bpy,** and **bpy,** respectively, ascribed to the extended conjugation of the **PhE_2-bpy** ligand**.** The spectra of the complexes display a broadband due to the π – π* transition of both primary antenna and ancillary ligands peaking at $\lambda_{\max}^{abs}$ = 311, 340 and 300 nm for **Eu-1**, **Eu-2** and **Eu-3,** respectively (**Fig. S14, ESI**). The spectra of **Eu-1** and **Eu-2** are redshifted by 11 nm and 40 nm, respectively, compared to **Eu-3**. The redshift of **Eu-2** is attributed to enhanced conjugation as the terminal bromines substituents have been replaced with the phenylethnyl groups with the longer wavelength transition leading to a lower probability of photobleaching [19].

To understand the results of the experimental optical absorption spectroscopy and the origin of the electronic transitions i.e., involvement of the molecular orbitals (MOs), we have calculated the absorption spectra (details are included in the **ESI**) and natural transition orbitals (NTOs) analysis is performed. **Figs. 1b – 1d** show theoretical absorption spectra calculated using the TD-DFT approach considering different density functionals and details of choosing an appropriate method is included in the ESI (Section 7.2).

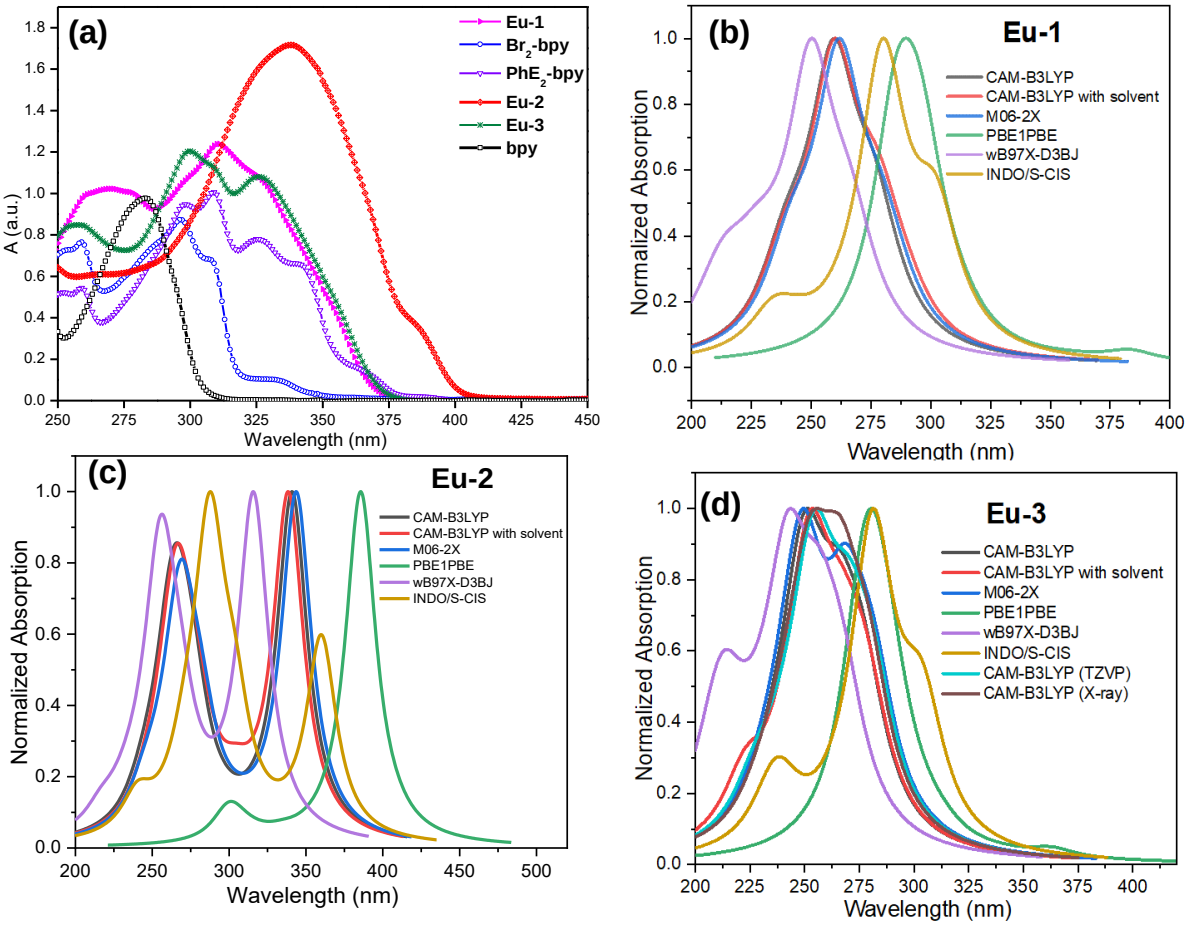

Fig. 1: (a) Experimental UV-Visible absorption spectra of the complexes and free ligands (bpy, Br_2-bpy and PhE_2-bpy) in CH_2Cl_2 solution at room temperature. Theoretical absorption spectra calculated by the TD-DFT method for the (b) **Eu-1,** (c) **Eu-2** and (d) **Eu-3** using different methods.

In this context, considering the CAM-B3LYP results and solvent effect for each complex, an analysis of the NTO was made **(Fig. 2)**. From this analysis a simple representation of the transition densities between the ground and the excited state is obtained. **Fig. 2** reveals that the most intense absorption band involved participation of both primary (btfa) and ancillary ligands for the three complexes. Furthermore, it is important to emphasize that the π→π* electronic transitions involved MOs energetically close to the highest occupied molecular orbital (HOMO) and lowest unoccupied molecular orbital (LUMO) frontier orbitals. In the case of **Eu-2**, the absorption band located at the highest wavelengths contains only the contribution from MOs centered on the **PhE_2-bpy** ligand. Furthermore, results obtained by INDO/S-CIS calculations are identical to the TD-DFT results and almost similar information can be extracted from the INDO/S-CIS results (**Fig. S15** and **Table S4**, **ESI**).

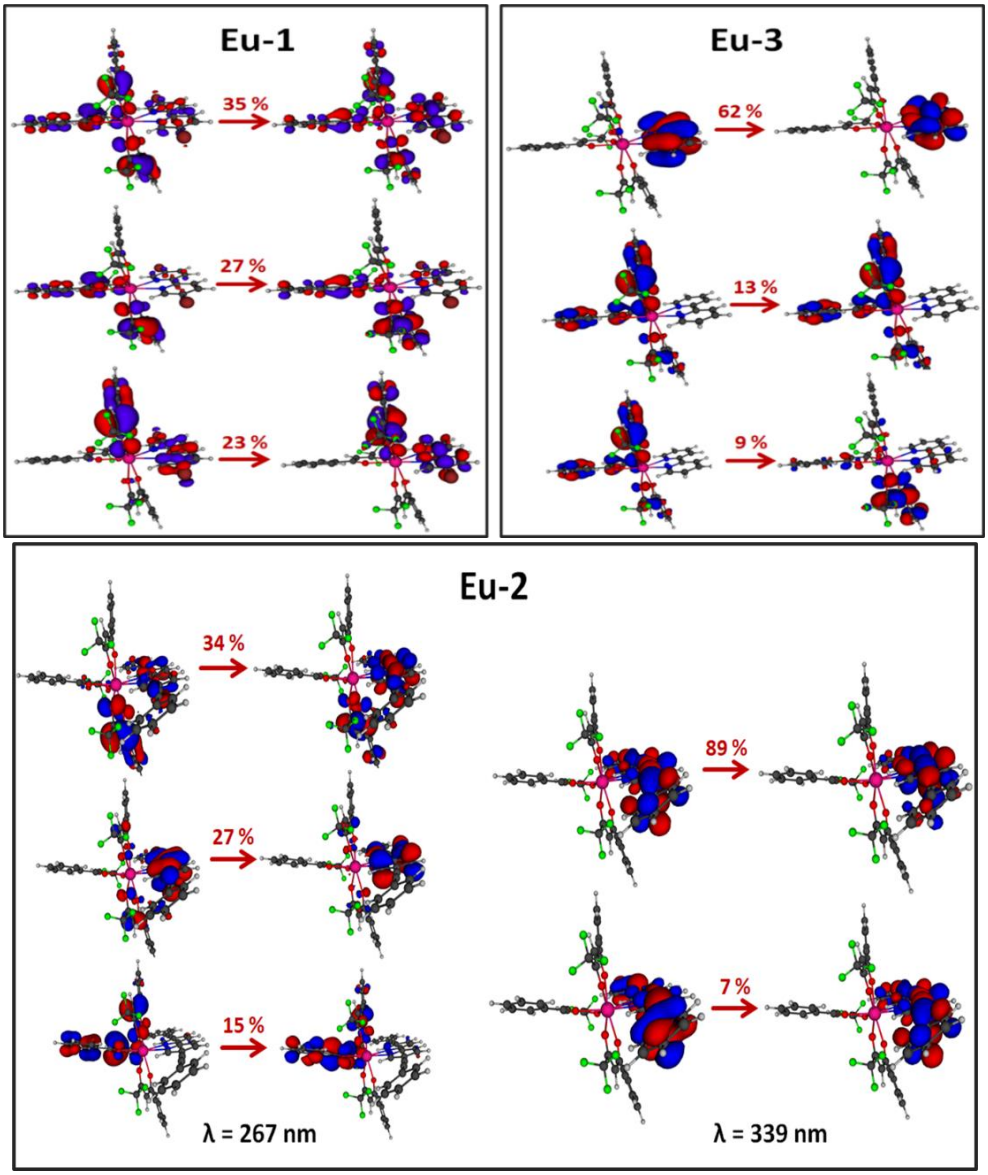

Fig. 2: Picture of the NTO mainly contributing to the singlet excited state with higher oscillator strength for **Eu-1, Eu-2** and **Eu-3**. The contribution percentages of the main NTO are also presented for each of the transitions.

To check the second requirement i.e., ΔE between the triplet state and emitting state of Eu(III), we have synthesized and characterized the gadolinium (Gd) complexes (**[Gd(NO$_3$)$_3$(Br$_2$-bpy)] (Gd-1)** and **[Gd(NO$_3$)$_3$(Ph$_2$-bpy)] (Gd-2)**, please see the experimental details in the **ESI**, **Section3**) as the emitting state $^6P_{7/2}$ state is situated at ~32,000 cm^{-1} and thus is too high to be populated by most of the organic ligand(s).[1d] For the **Eu-1** and **Eu-2** complexes**,** the primary antenna ligand is the same having a triplet state ~ 21,400 cm^{-1} [20] and is well above (2,373 and 4,107 cm^{-1}) the receiving states $^5D_1$ (19,027 cm^{-1}) and $^5D_0$ (17,293 cm^{-1}) of Eu(III) ion [21]. To determine ΔE between the T_1 of the ancillary ligands and the receiving states of the Eu(III) ion, we utilized the **Gd-1** and **Gd-2** complexes and monitored their

phosphorescence spectra at 77K (**Fig. S16** & **S17**, **ESI**) and found the triplet state of the ancillary ligands are at ~ (21,645 cm^{-1})$_{Br2\text{-}bpy}$ and (19,305 cm^{-1})$_{Ph2\text{-}bpy}$, respectively. The calculated ΔE for **Eu-1** ~ (2,618 and 4,352 cm^{-1}) and **Eu-2** ~ (2,78 and 2,012 cm^{-1}) suggest that the emission of **Eu-1** would be more efficient than for **Eu-2**.

3.2.2. PL Studies

The excitation and emission spectra of the complexes under investigation were determined in CH_2Cl_2 solution at room temperature. The excitation spectra of the complexes were obtained by fixing on the strongest emission peak $^5D_0 \rightarrow {}^7F_2$. The spectra in each case displayed broad bands in the region between 350 and 500 nm (**Fig. S18, ESI**) and could be assigned to π-π* transitions of both the btfa and ancillary ligands with a very faint intraconfigurational f – f transition $^7F_0 \rightarrow {}^5D_2$ at 465 nm [22]. Moreover, in each case, the excitation spectrum is dominated by the broad ligand absorption band. It is worth noting that the excitation spectrum of **Eu-2** extends into the visible blue region with λ_{max}^{Ex} = 408 nm which is approximately 35 nm redshifted (**Fig. S18, ESI**) compared to **Eu-1** (λ_{max}^{Ex} = 373 nm) and **Eu-3** (λ_{max}^{Ex} = 376 nm). The redshifted excitation window is attributed to the extended conjugation which is provided by phenylethnyl group of the chromophore.

The PL spectra of the complexes were obtained by exciting them at λ_{max}^{Ex} = 376, 373 and 406 nm for **Eu-1**, **Eu-3** and **Eu-2**, respectively. The data obtained such as peak positions, relative intensity and % contribution of each transition is collected in **Table S5, ESI**. The spectra of the complexes exhibit typical Eu(III) emission transitions emanating from the $^5D_0$ state to ^7F_J (J = 0, 1, 2, 3 and 4) in the region between 570 – 720 nm (**Fig. 3**). Apart from the Eu(III) emission transitions the spectrum of **Eu-2** displays ligand fluorescence in the region between 400 nm and 560 nm. The presence of ligand fluorescence in the spectrum of **Eu-2** could be due to energy mismatch (2,780 and 2,012 cm^{-1}) between the receiving state and triplet state of the ancillary **PhE$_2$-bpy** ligand. The spectra in each case are dominated by the narrow (FWHM = 4.48 – 6.58 nm, **Table 1**) electric-dipole (ED) $^5D_0 \rightarrow {}^7F_2$ with the total integral intensity of 82.00 – 78.32%. Furthermore, we have calculated the CIE color coordinates (**Table 1**) of the complexes from the emission spectra. **Eu-1** and **Eu-3** exhibited highly monochromatic red emission (**Fig. S19, ESI**) with the (CIE)$_{Eu\text{-}1}$ = 0.607; 0.329 and (CIE)$_{Eu\text{-}3}$ = 0.668; 0.328 while **Eu-2** displays pinkish-red color [(CIE)$_{Eu\text{-}3}$ = 0.498; 0.233, **Fig. S19, ESI**] due to the presence of blue ligand fluorescence. The dominant highly monochromatic red color from **Eu-1** and **Eu-3** complexes imply that they have the potential to be utilized as EML to fabricate R-OLEDs. Moreover, they could also be used as a red-light emitting component in the fabrication of tricolor RGB (red, green, and blue) based white OLEDs. Furthermore, the dominant nature of the ED $^5D_0 \rightarrow {}^7F_2$ transition over the magnetic-dipole (MD) $^5D_0 \rightarrow {}^7F_1$ transition implies that forced ED and the dynamic coupling (DC) mechanism are dominant over MD.[10f, 23]

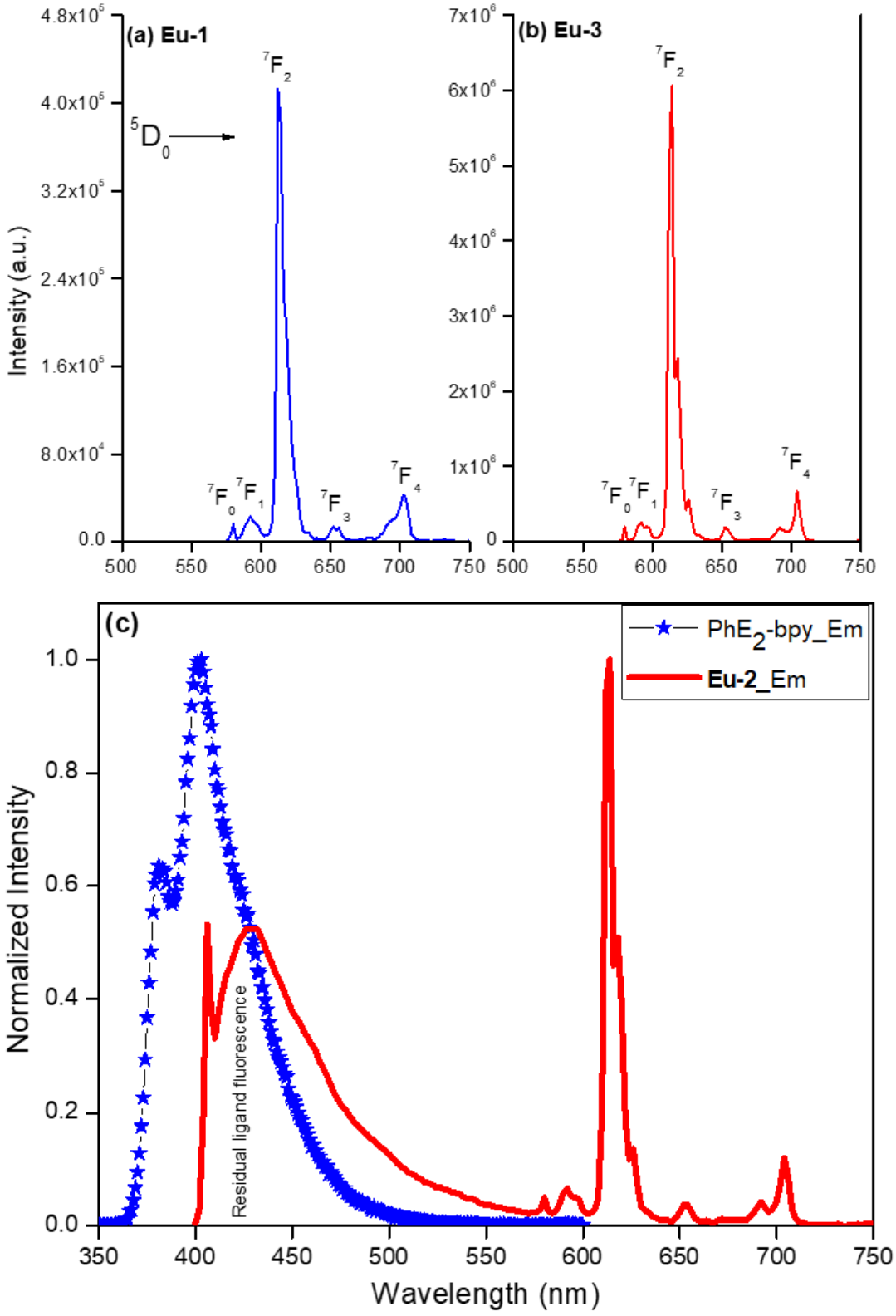

Fig. 3. Room temperature emission spectra of (a) **Eu-1** and (b) **Eu-3** (c) **PhE$_2$-bpy** and **Eu-2** in CH_2Cl_2.

Table 1: Experimental and theoretical photophysical parameters of the mixed ligand complexes **Eu-1, Eu-2 and Eu-3** at room temperature.

Complexes	Ω_2	Ω_4	FWHM[b]	τ_{obs}	τ_{rad}	A_R	A_{NR}	Q_{Eu}^{Eu}	Q_{Eu}^{L}	R_{21}	η_{sen}	$CIE_{(x,y)}$
	$\times 10^{-20}$ cm^2		(nm)	(μs)		(s^{-1})		(%)			(%)	
Eu-1	26.19[a]	10.15[a]	6.58	815.56	1147[c]	871.69[d]	355.31[d]	71.04[e]	40.00	14.85	56.30[f]	0.668; 0.336
Theoretical	26.18	10.15	-	-		843.41	382.74	68.79	40.44	-	58.79	-
Eu-2	20.47[a]	7.70[a]	5.06	415.15	1492[c]	690.70[d]	1713.14[d]	28.73[e]	16.00	11.55	55.69[f]	0.498; 0.233
Theoretical	20.47	7.70	-	-	-	665.61[d]	1734.16	27.63	16.05	-	58.08	-
Eu-3	30.25[a]	9.91[a]	4.48	926.91	1024[c]	975.76[d]	102.99[d]	90.45[e]	63.00	17.27	69.65[f]	0.674; 0.331
Reported[14]	-	-	-	-	-	-	-	-	65.00	-	-	-
Theoretical	30.24	9.90	-	-		944.07	134.78	87.51	59.99	-	68.56	-

[a]Calculated using eqn (S1); [b]Full width at half maxima of the $^5D_0 \rightarrow {}^7F_2$ transition; [c]calculated using eqn (S5); [d]calculated using eqn S2 – S4; [e]calculated using eqn (S6); [f]calculated using eqn (S7)

3.2.3. J–O parameters, excited-state lifetime, rate constants, PLQY and ET mechanism

To present a clear picture of the effect of different bipyridine-based ancillary ligands on the photophysical properties, we have determined the important photophysical parameters. These include luminescence lifetime (τ_{obs}), J-O intensity parameters (Ω_2 and Ω_4), A_R, A_{NR}, natural radiative lifetime (τ_{rad}), Q_{Eu}^{Eu}, Q_{Eu}^{L} and sensitization efficiency (η_{sen}) of the newly synthesized **Eu-1** and **Eu-2**. We have also determined the above-mentioned properties of **Eu-3** for which these important photophysical parameters have not been reported [14] previously except for the Q_{Eu}^{L}. The photophysical properties were calculated utilizing equation S1 – S7, **ESI** (**Table 1)**. PL decay curves of Eu(III) complexes are recorded for the $^5D_0 \rightarrow {}^7F_2$ transition and pulsed excitation and fits satisfactorily to a mono-exponential decay (χ^2 = 1.01–1.15, **Fig. S20 – Fig. S22, ESI**). This substantiates the presence of a single dominant emitting species and attests to the results of the steady-state measurement where the singlet emission transition $^5D_0 \rightarrow {}^7F_0$ (17241 cm^{-1}, **Table S5, ESI**) displays a single emission peak. A comparison of the τ_{obs} of the complexes gives the following order: **Eu-3** (926.94 µs) > **Eu-1** (816.56 µs) > **Eu-2** (415.54 µs). Moreover, the τ_{obs} value of the present complexes are 5.27, 4.64 and 2.57 and are higher than the [Eu(btfa)$_3$(H$_2$O)$_2$] hydrated complex (175.66 µs) [1b]. This could be related to the substitution of water molecules by the ancillary ligands (**Br$_2$-bpy**, **PhE$_2$-bpy** and **bpy**) in the coordination sphere, which in turn decreases the A_{NR} values from 4853.38 s^{-1} [1b] to 102.99 – 355.31 s^{-1} (**Table 1**). This is further reflected in the Q_{Eu}^{Eu} value and follows the similar order **Eu-3** (90.45%) **> Eu-1** (71.04%) **> Eu-2** (28.73 %) as noted for τ_{obs}. Ω_2 and Ω_4, that were determined from the emission spectra and resultant data are shown in **Table 1**. The high value of the Ω_2 = 26.19×10^{-20} cm^2, 20.47×10^{-20} cm^2, and 30.25×10^{-20} cm^2, respectively for **Eu-1**, **Eu-2**, and **Eu-3** jointly with the high R_{21} (17.27 – 14.85, **Table 1**) implies that the Eu(III) ion in the complexes are in a highly polarizable chemical environment (strong delocalization of the β-diketonate oxygen charge). The parameter Ω_4 is related to long-range effects (hydrogen bonding, π– π stacking) or rigidity and its high values suggest that the complexes perhaps display these features [19]. The complexes exhibit large values and follows the order **Eu-1** (10.15×10^{-20} cm^2) > **Eu-3** (9.91×10^{-20} cm^2) > **Eu-2** (7.70×10^{-20} cm^2). A comparison of the values suggests that these effects are more pronounced in **Eu-1** and could be due to the presence of the bromine (Br) atom (potential hydrogen bonding moiety) in the ancillary **Br$_2$-bpy** ligand. The Q_{Eu}^{L} in solution is calculated and the complexes **Eu-3** (63.00%) and **Eu-1** (40.00%) exhibited large values while **Eu-2** displayed a lower value than both the

complexes in agreement with the experimental energy gap for **Eu-2** ~ (2,780 and 2,012 cm^{-1}). This leads to a substantially large value of A_{NR} = 1713.14 s^{-1} compared to the **Eu-1** (A_{NR} = 355.31 s^{-1}) and **Eu-3** (A_{NR} = 102.99 s^{-1}). **Table 1** shows that the intensity parameters calculated using the DFT geometries resulted in values in agreement with the experimental ones. As a result, the theoretical and experimental A_R are concordant. In addition, the binary outcome acceptance attribute for the adjustment represented by the *D*/*C* value (**Table S6, ESI**) is larger than 1.0 for the three complexes, indicating that the experimental J-O intensity parameters were well adjusted by the *QDC* model. By means of this model, the forced ED intensity parameters (Ω_λ^{FED}) contained in **Table S6 (ESI)** were obtained, Ω_λ^{FED} is important to calculate the contribution due to the direct Coulombic interaction (CI) mechanism **(Eq. S8)** for the ET rates.

As can be seen in **Table S7, ESI**, the lowest triplet state energy of the **Eu-1** and **Eu-3** complexes calculated by the different levels of theory are similar, suggesting that the presence of the Br substituent of the **bpy** ligand did not play any significant role in changing the electronic structure related to T_1. Thus, it is expected that the ET rates for the pathways involving T_1 will be quite similar for both complexes (**Eu-1** and **Eu-3**). However, **Eu-2** revealed a lower T_1 value compared to **Eu-1** and **Eu-3** because the extended conjugation of the phenylethynyl groups imparted additional stability to the complex. **Table S8** lists the contributions of the electronic transitions calculated at the CAM-B3LYP/SVP/MWB52 level of theory for the T_1 composition of the three complexes. In the case of **Eu-1** and **Eu-3**, MOs centered on both primary and ancillary ligands are involved with the T_1 composition (**Fig. 4**). For instance, the experimental determination revealed that the T_1 of btfa (21,400 cm^{-1}) was almost similar to the respective state of **Br_2-bpy** (21,645 cm^{-1}). Consequently, it is expected that the T_1 contains contributions from both ligands in the complexes, as indicated by the TD-DFT result. In case of **Eu-2**, the phosphorescence spectra of **Gd-2** at 77 K provided energy of 19,305 cm^{-1} for T_1. As this value is much lower than the energy related to the btfa ligand, it is probable that T_1 in **Eu-2** has a larger contribution from the **PhE_2-bpy** ligand. Thus, the TD-DFT results indicated that the HOMO→LUMO transition is the most important one for T_1 and both the MOs are centered on the ancillary **PhE_2-bpy** ligand (**Fig. 4**). In addition, **Table S8** shows that the second lowest triplet (T_2) of **Eu-2** contained only contributions from MOs centered on the btfa ligands, this state was around 1,500 cm^{-1} above T_1. Therefore, the theoretical results are qualitatively in perfect agreement with the experimental observations.

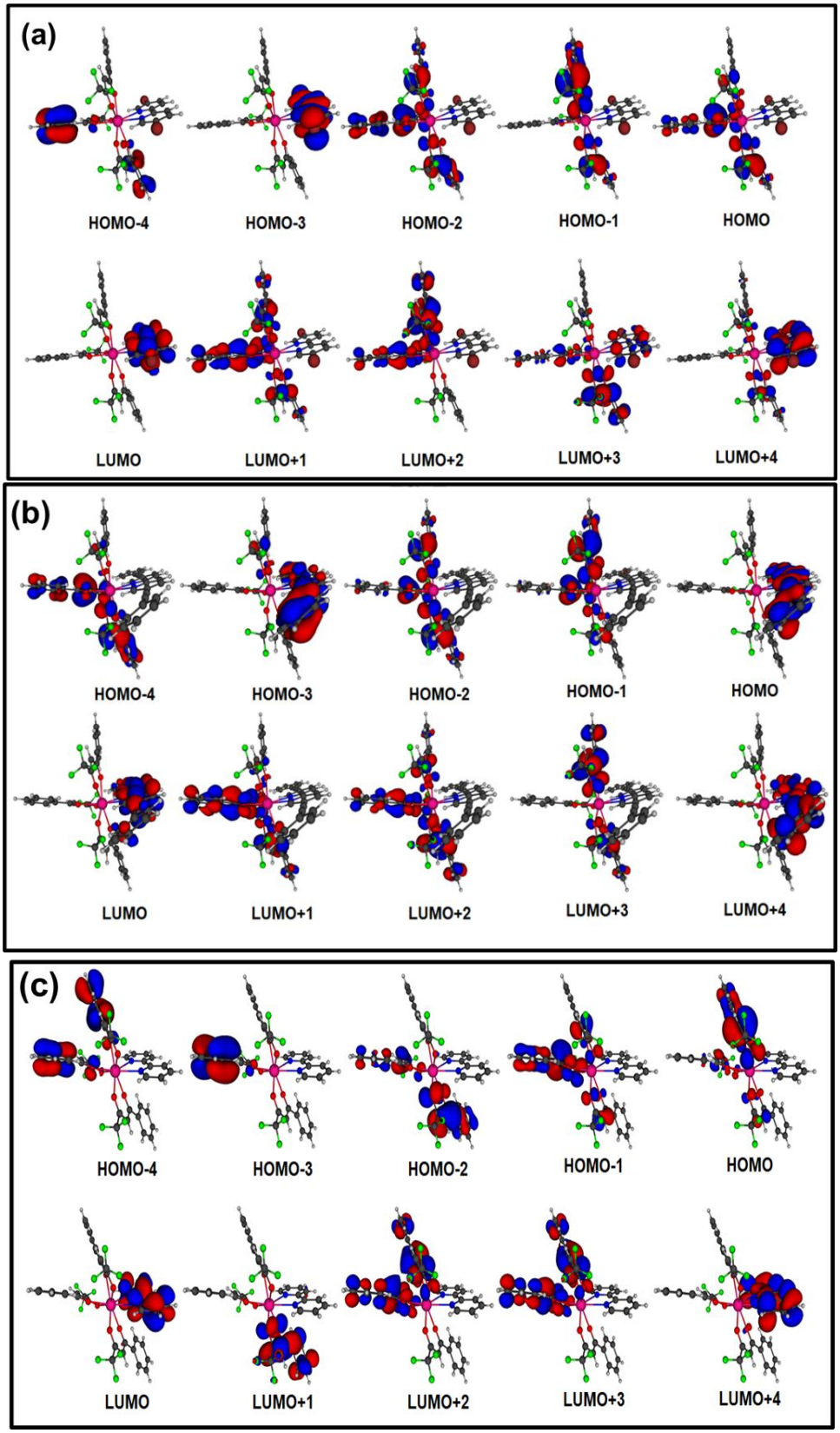

Fig. 4. MOs in the range from HOMO-4 to LUMO+4 calculated at the CAM-BL3LYP/SVP/MWB52 level of theory, considering the PBE1PBE geometries and the effect of the DCM solvent implicitly, for (a) **Eu-1**, (b) **Eu-2** and (c) **Eu-3**.

Table 3: Ligand-metal energy transfer rates calculated using Malta's model for **Eu-1**, **Eu-2**, and **Eu-3** considering the CAM-B3LYP results.

ET pathway	**Eu-1** q^{calc} = 40.4 % η_{sen}^{calc} = 58.8 %		**Eu-2** q^{calc} = 16.0 % η_{sen}^{calc} = 58.1 %		**Eu-3** q^{calc} = 60.0 % η_{sen}^{calc} = 68.6 %	
	W_{ET} (s^{-1})	W_{BT} (s^{-1})	W_{ET} (s^{-1})	W_{BT} (s^{-1})	W_{ET} (s^{-1})	W_{BT} (s^{-1})
$S_1 \rightarrow {}^5D_4$	3.49×10^{4}	2.56×10^{-9}	5.94×10^{3}	4.98×10^{-1}	4.86×10^{4}	9.21×10^{-9}
$T_1 \rightarrow {}^5D_1$	4.06×10^{7}	2.95	1.60×10^{6}	8.84×10^{1}	6.13×10^{7}	6.01
$T_1 \rightarrow {}^5D_0$	1.01×10^{8}	1.80×10^{-3}	5.47×10^{6}	7.39×10^{-2}	1.55×10^{8}	3.71×10^{-3}
$T_2 \rightarrow {}^5D_1$	-	-	3.53×10^{7}	2.24		
$T_2 \rightarrow {}^5D_0$	-	-	8.75×10^{7}	1.36×10^{-3}		

The most important ET pathways calculated using models proposed by Malta are shown in **Fig. 5**. Since the excited states of **Eu-1** and **Eu-3** were similar and the lowest triplet states showed the contribution of MOs centered on the btfa and ancillary ligands, a common schematic energy diagram is proposed, i.e., only the presence of T_1 was considered. On the other hand, the inclusion of T_1 and T_2 in the ET pathways of **Eu-2** highlights the contribution of the btfa and **PhE_2-bpy** ligands in the ET process. The CAM-B3LYP results, including the effect of solvent, were used to quantify the ET rates considered in the ET process of the complexes (**Table 3**). The $T_1 \rightarrow {}^5D_0$ and $T_1 \rightarrow {}^5D_0$ transitions assumed equal importance to sensitize the Ln ion in the complexes, being the ${}^5D_0 \leftarrow {}^7F_0$, ${}^5D_0 \leftarrow {}^7F_1$, ${}^5D_1 \leftarrow {}^7F_0$, and ${}^5D_1 \leftarrow {}^7F_1$ electronic excitations associated with these transitions, which are governed by the Ex. mechanism. The ${}^5D_0 \leftarrow {}^7F_0$ transition can occur due to a *J*-mixing involving the ${}^7F_0$ and ${}^7F_2$ states (*ca*. 5%).[24] Additionally, the thermal population of the ${}^7F_0$ and ${}^7F_1$ states in the calculations were considered equal to 0.64 and 0.33 at 300 K, respectively. Because the PhE_2-bpy ligand has a larger dimension than the other ancillary ligands, the distance between the energy barycenter of T_1 and the states centered on Eu(III) assumed a larger value, and consequently, the ET rates related to T_1 resulted in the lowest values. As shown in **Table 1**, η_{sen} assumed values of 56% and 69% for **Eu-1** and **Eu-3**, respectively, and these values may suggest that non-radiative decay from T_1 is operative in each case, reducing the efficiency of population of the ${}^5D_0$ emitting level of the Eu(III) ion. In this context, the order of magnitude of the $S_1 \rightarrow T_1$ and $T_1 \rightarrow S_0$ rates was adjusted to reproduce the experimental η_{sen}. Therefore, the values of 10^7 s^{-1} and 10^8 s^{-1} for $S_1 \rightarrow T_1$ and $T_1 \rightarrow S_0$, respectively, resulted in calculated η_{sen} for **Eu-1** (58.8 %) and **Eu-3** (68.6 %), which are in excellent agreement with those experimentally observed. Since **Eu-1** and **Eu-3** had all rates with the same order of magnitude, the largest sensitization efficiency of **Eu-3** is due to the largest corresponding value of A_R. In the case of

Eu-2, rate values of 10^8 s^{-1} for the $S_1 \rightarrow T_2$, $T_2 \rightarrow T_1$ and $T_1 \rightarrow S_0$ transitions provided calculated η_{sen} equalling to 58%, which is in good agreement with the experimental value (56%, **Table 1**).

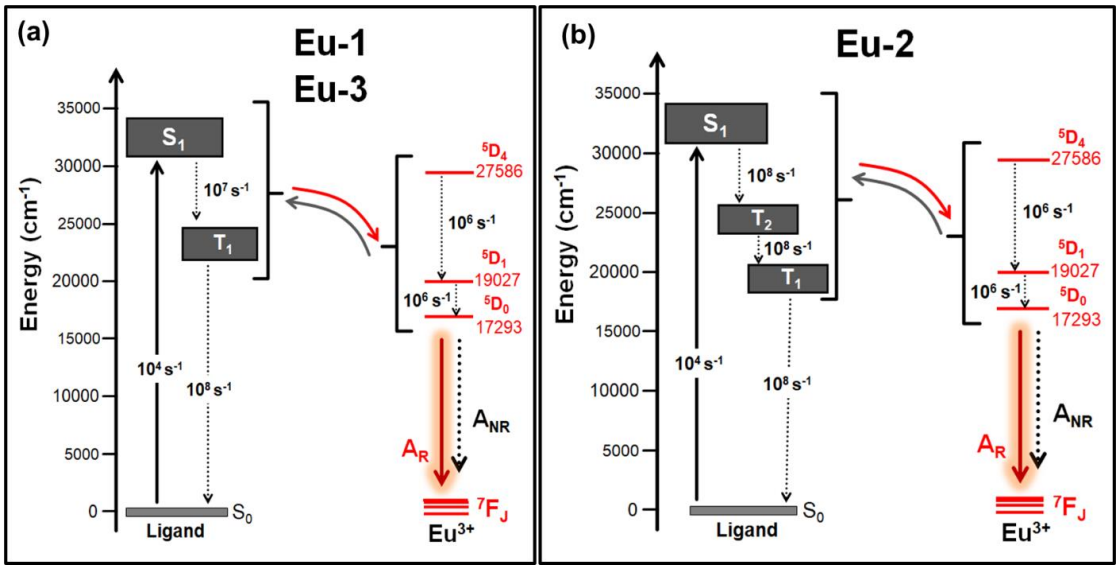

Fig. 5. Schematic energy-level diagram proposed for **Eu-1**, **Eu-2**, and **Eu-3.**

3.3. Fabrication and measurement of red OLEDs

The impressive photophysical properties (**Table 1**) and excellent thermal stability (Please see the discussion in Section 7.3 and Fig. S23, ESI) of the **Eu-3** motivated us to utilize it as a red emitter to fabricate single- and double-EMLs red OLEDs with the following general device configuration: **single-EML**: ITO/HAT-CN (23 nm)/TAPC(70 nm)/**Eu-3**(x%):26DCzPPy (10 nm)/Tm3PyP26PyB (60 nm)/LiF (1 nm)/Al (200 nm) and **double-EMLs**: ITO/HTA-CN(23 nm)/TAPC(70 nm)/**Eu-3** (8%):TCTA (10 nm)/**Eu-3**(x%):26DCzPPy (10 nm)/Tm3PyP26PyB (60 nm)/LiF (1 nm)/Al (200 nm) by thermal evaporation under high vacuum (HAT-CN = Dipyrazino[2,3-f:2'3'-h]quinoxaline-2,3,6,7,10,11-hexacarbonitrile; 26DCzPP = 2,6-bis[3-(9H-Carbazol-9-yl)phenyl]pyridine; Tm3PyP26PyB = 1,3,5-tris(6-(3-(pyridin-3-yl)phenyl)pyridin-2-yl)benzene; TCTA = 4,4',4"-tris(carbazol-9-yl)triphenylamine). The doping concentrations of **Eu-3** were regulated to be 4.0 wt%, 6.0 wt%, 8.0 wt%, 10.0 wt% and 12.0 wt% respectively, in different devices. The evaporation temperature increases gradually from 139 to 153 °C as the doping concentration increases. The low thermal evaporation temperature of **Eu-3** thus ensures negligible decomposition during the thermal evaporation process.

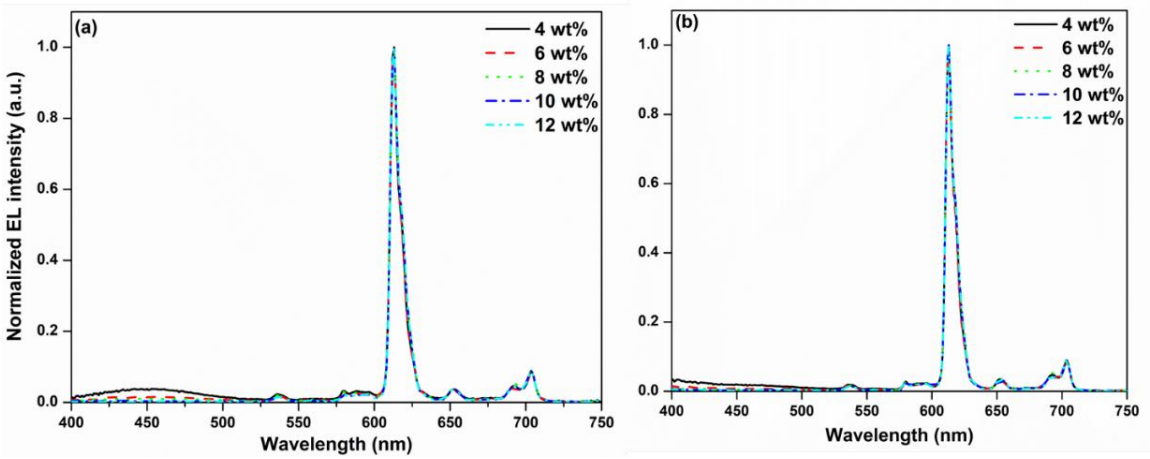

Fig. 6. Normalized EL spectra of single and double EML devices (a) **devices 1–5** and (b) **devices 6–10** of **Eu-3** operating at 10 mA/cm^2.

EL spectra of **Eu-3** based single- as well as double-EML(s) OLEDs exhibit similar emission profiles as observed in the steady-state PL (550 – 750 nm, **Fig. 6**). The EL also showed very minor host emission from 400 – 500 nm whose intensity decreases as the doping concentration increases implying the ET from the host to **Eu-3** becomes more efficient i.e., (Devices **4** and **5**) since a greater quantity of **Eu-3** is contributing to the luminescence processes and thus emitting pure red emission with $(CIE)_{x,y}$ colour coordinates of (**Device 4**: x= 0.621,y = 0.320 and **Device 5**: x= 0.629,y = 0.321). The double-EMLs device with the TcTa host in conjunction with the 26DCzPPy host displayed similar sharp EL profiles in the region between 550 – 750 nm, which is dominated by the red emission transition $^5D_0 \rightarrow {}^7F_2$ at 614 nm (**Fig 6b**). Interestingly, the double-EMLs device does not display any host emission suggesting an improved ET efficiency from the host to **Eu-3**. Moreover, these observations clearly advocate that in the device luminescence process, both carrier trapping and Förster ET are taking place simultaneously [25]. The EL efficiency and current density curves, together with the voltage (V)-brightness (B) and current density curves as an inset are shown in **Fig. 7** and data obtained such as B, current efficiency (η_c), power efficiency (η_p) and external quantum efficiency (EQE) are shown in **Table 4**. Single-EML devices at the optimum doping concentration, i.e., **Device 4 (**10 Wt%) displayed B = 291 cd/m^2, η_c = 2.91 cd/A, η_p = 1.87 lm/W with an EQE = 1.27 % at very low $V_{turn\text{-}on}$ = 3.4 V with (CIE)x,y = 0.621; 0.320 at current density = 10 mA/cm^2. The double-EMLs device at the optimum doping concentration of 8.0 wt% (**Device 8**) displayed an impressive EL performance B = 428 cd/m^2, η_c = 3.31 cd/A, η_p = 3.06 lm/W, and EQE = 2.14% at very low $V_{turn\text{-}on}$ = 3.4 V with (CIE)x,y = 0.619, 0.323 at current density = 10 mA/cm^2. The EQE value of the **Eu-3** based R-OLEDs is higher than than that of $[Eu(tta)_3(Phen)]$ [26] and compares well with the reported efficient complexes $[Eu(tta)_3(Dppz)]$ [25a], $[Eu(dbm)_3(Phen)]$ [27], $[Eu(tta)_3(DPEPO)]$ [28], $[Eu(btfa)_3(Py\text{-}Im)]$ [1a], $[Eu(dbm)_3(Ox\text{-}Py\text{-}Im)]$ [25b] (tta = thenoyltrifluoroacetone; dbm = Dibenzoylmethane; btfa = 4,4,4-trifluoro-1-

phenyl-1,3-butanedione; Dppz = dipyrido[3,2-a:2′,3′-c]phenazine; DPEPO = bis(2-(diphenylphosphino)phenyl) ether oxide; Py-Im = 2-(2-pyridyl)benzimidazole, Ox-Py-Im = 2-phenyl-5-(4-(4-(2-(pyridin-2-yl)-1H-benzo[d]imidazole-1-yl)butoxy)phenyl)-1,3,4-oxadiazole). Furthermore, the low $V_{turn-on}$ implies barrier-free carrier injection, balanced carrier transport and recombination and as well as high ET efficiency from the exciplex host to **Eu-3**. Moreover, η_c increases from Device **6** to Device **8** and then a decrease is observed and could be due to the hole-electron pair imbalance in the EML layer. Hence it will break this balance and thus would lead to the decrease of the η_c of the device. Moreover, in all the cases, the double-EMLs devices displayed monochromatic red emission close to the standard (NTSC; 0.67, 0.33) suggesting its potential to be utilized as a red component in the traditional RGB approach to produce full-color display panels in portable devices.

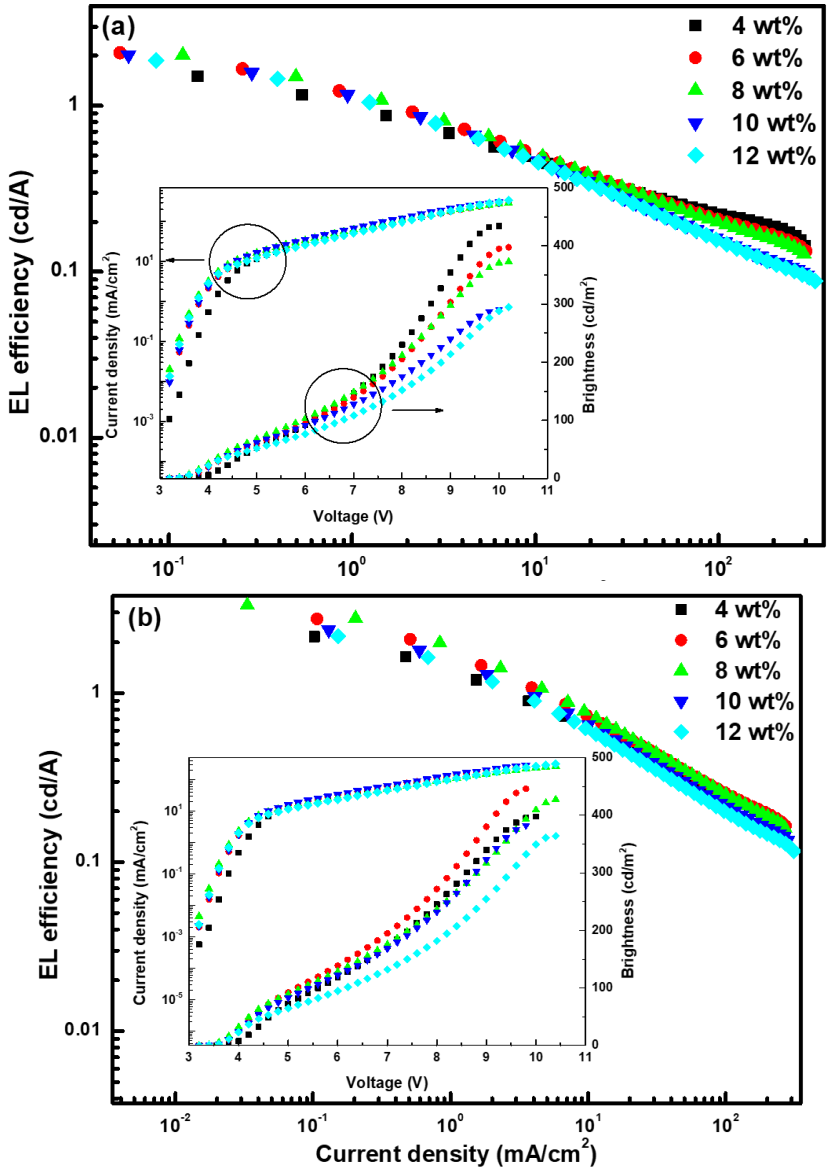

Fig. 7: EL efficiency-current density characteristics of the devices. Inset: Current density-brightness-voltage characteristics of devices. (a) **devices 1–5** and (b) **devices 6–10** of **Eu-3.**

Table 4: Key properties of single- and double-EML(s) EL devices of **Eu-3**.

	$V_{turn-on}$ (V)	B[a] (cd/m^2)	η_c[b] (cd/A)	η_p[c] (lm/W)	EQE(%)[d]	$CIE_{x,y}$[e]
Single EML Devices						
Device 1 (4 wt%)	3.8	434	1.50	1.24	0.93	(0.572, 0.335)
Device 2 (6 wt%)	3.4	398	2.08	1.92	1.3	(0.592, 0.327)
Device 3 (8 wt%)	3.4	249	2.02	1.87	1.26	(0.614, 0.320)
Device 4 (10 wt%)	3.4	291	2.91	1.87	1.27	(0.621, 0.320)
Device 5 (12 wt%)	3.4	295	1.87	1.73	1.16	(0.629, 0.321)
Double EMLs Devices						
Device 6 (4 wt%)	3.8	398	2.16	1.78	1.33	(0.588,0.323)
Device 7 (6 wt%)	3.6	446	2.75	2.40	1.70	(0.602,0.322)
Device 8 (8 wt%)	3.4	428	3.31	3.06	2.14	(0.619,0.323)
Device 9 (10 wt%)	3.6	382	2.37	2.07	1.45	(0.625,0.320)
Device 10 (12 wt%)	3.6	364	2.17	1.89	1.34	(0.631,0.317)

[a]The data for maximum brightness (B), [b]maximum current efficiency (η_c), [c]maximum power efficiency (η_p); [d]maximum external quantum efficiency (EQE),[e]$CIE_{x,y}$ at 10 mA/cm^2

Conclusion

In summary, we have successfully synthesized two new ternary **Eu-1** and **Eu-2** complexes together with the previously reported **Eu-3** complex. Photophysical properties of the complexes were determined experimentally and further complemented by the theoretical calculations. The absorption spectra of the complexes display a strong broad band in the region 300 – 350 nm due to the π – π* transition of both ligands, which is further confirmed by the NTO analysis. Moreover, $\lambda_{\max}^{abs}$ of **Eu-2** is redshifted due to enhanced conjugation arising from substitution of the terminal bromine atoms in **Eu-1** by the phenylethynyl groups. PL properties displayed typical highly monochromatic Eu(III) red emissions for **Eu-1** and **Eu-3** while **Eu-2** exhibited pinkish-red color due to the presence of blue RFL. This is due to very small ΔE between the emitting state and triplet state of the ancillary ligand in **Eu-2** that resulted in a large A_{NR} = 1713.14 s^{-1} compared to the **Eu-1** (A_{NR} = 355.31 s^{-1}) and **Eu-3** (A_{NR} = 102.99 s^{-1}) and thus decreases the Q_{Eu}^{L}. The theoretical calculations are in line with the experimental results. The presence of Br on both rings of the bpy ligand did not play any significant in changing the electronic structure of T_1 However, replacement of terminal Br by phenylethynyl in the case of **Eu-2** results in a lowering of triplet state energy (19,305 cm^{-1}) and TD-DFT results indicated that the HOMO→LUMO transition is the most important one for T_1 and both the MOs are centred on the ancillary **PhE_2-bpy** ligand. It is important to note that acetylide functionalized heterocyclic ligand(s) have not been explored in lanthanide coordination

chemistry though polymetalla-yne type of ancillary ligands have been used to sensitize the visible and near infrared (NIR) emission of Ln(III) ion. The work presented herein will open the gateway to explore the potential of a broad range of poly-yne type primary or ancillary ligands to sensitize visible and NIR emission of Ln(III) ion. the ET mechanism for **Eu-1** and **Eu-3** are similar where only T_1 is involved with the contribution from both primary and ancillary ligands. While the ET process for **Eu-2** utilizes T_1 centred on PhE_2-Bpy ($T_1 \rightarrow {}^5D_1$ = 1.60×10^6 s^{-1} and $T_1 \rightarrow {}^5D_0$ = 5.47×10^6 s^{-1}) and T_2 centred on the btfa ligand ($T_2 \rightarrow {}^5D_1$ = 3.53×10^7 s^{-1} and $T_2 \rightarrow {}^5D_0$ = 8.75×10^7 s^{-1}). Finally, the complex (**Eu-3**) was chosen as an EML to fabricate R-OLEDs. The EL performance at the optimum doping concentration for the double EMLs device (**Device 8**) displayed bright red EL at current density = 10 mA/cm^2 with the EQE of 2.14% and B = 428 cd/m, η_c = 3.31 cd/A, η_p = 3.06 lm/W at very low $V_{turn\text{-}on}$ = 3.4 V, suggesting it as a strong candidature in the fabrication of tricolor RGB based white OLEDs.

Conflict of Interests

The authors declare no conflict of interest.

Acknowledgements

MSK acknowledges His Majesty's Trust Fund for Strategic Research (Grant No. SR/SQU/SCI/CHEM/21/01) and The Ministry of Higher Education, Research and Innovation (MoHERI), Oman (Grant: RC/RG-SCI/CHEM/20/01) for funding. IJAB thanks Ministry of Education, Sultanate of Oman (MOE) for a Ph.D. scholarship. R. I. thanks His Majesty's Trust Fund for a postdoctoral fellowship. JDLD appreciates the financial support from the Brazilian funding agencies: CAPES, CNPq (421733/2018-7), FACEPE (APQ - 0675-1.06/14) and FAPITEC-SE (Process N. 019.203.01074/2011-1). WFO thanks PIBIC/CNPq/UFS for a scientific initiation fellowship. The computing for this project was performed on the LCAD-UFS (UFS High Performance Computing Laboratory). WYW thanks the Hong Kong Research Grants Council (PolyU 153058/19P), Guangdong-Hong Kong-Macao Joint Laboratory of Optoelectronic and Magnetic Functional Materials (2019B121205002), Hong Kong Polytechnic University (1-ZE1C), Research Institute for Smart Energy (RISE) and the Endowed Professorship in Energy from Ms Clarea Au (847S) for the financial support. LZ is grateful to the financial aid from National Natural Science Foundation of China (21771172), Youth Innovation Promotion Association of Chinese Academy of Sciences (2013150). PRR is grateful to the Engineering and Physical Sciences Research Council (EPSRC) for continued funding (Grant EP/K004956/1).

References

[1] (a) R. Ilmi, Zhang D., Dutra J. D. L., Dege N., Zhou L., Wong W.-Y., Raithby P. R., Khan M. S. A tris β-diketonate europium(III) complex based OLED fabricated by thermal evaporation method displaying efficient bright red emission. Org Electron. 96 (2021), p.p.106216; (b) R. Ilmi, Sun W., Dutra J. D. L., Al-Rasbi N. K., Zhou L., Qian P.-C., Wong W.-Y., Raithby P. R., Khan M. S. Monochromatic red electroluminescence from a homodinuclear europium(iii) complex of a β-diketone tethered by 2,2′-bipyrimidine. J Mater Chem C. 8 (2020), p.p.9816-27; (c) R. Ilmi, Kansız S., Al-Rasbi N. K., Dege N., Raithby P. R., Khan M. S. Towards white light emission from a hybrid thin film of a self-assembled ternary samarium(iii) complex. New J Chem. 44 (2020), p.p.5673-83; (d) R. Ilmi, Khan M. S., Li Z., Zhou L., Wong W.-Y., Marken F., Raithby P. R. Utilization of Ternary Europium Complex for Organic Electroluminescent Devices and as a Sensitizer to Improve Electroluminescence of Red-Emitting Iridium Complex. Inorg Chem. 58 (2019), p.p.8316-31; (e) T. Gong, Sui Q., Li P., Meng X.-F., Zhou L.-J., Gao E.-Q., Chen J., Xu J., Wang L. Versatile and Switchable Responsive Properties of a Lanthanide-Viologen Metal-Organic Framework. Small. 15 (2019), p.p.e1803468.

[2] (a) S. I. Weissman. Intramolecular Energy Transfer The Fluorescence of Complexes of Europium. J Chem Phys. 10 (1942), p.p.214-7; (b) G. A. Crosby, Whan R. E., Alire R. M. Intramolecular Energy Transfer in Rare Earth Chelates. Role of the Triplet State. J Chem Phys. 34 (1961), p.p.743-8; (c) N. Sabbatini, Guardigli M., Manet I. Chapter 154 Antenna effect in encapsulation complexes of lanthanide ions. In: Karl A. Gschneidner, Jr., LeRoy E, editors. Handbook on the Physics and Chemistry of Rare Earths: Elsevier; 1996. p. 69-119.

[3] M. Latva, Takalo H., Mukkala V. M., Matachescu C., RodriguezUbis J. C., Kankare J. Correlation between the lowest triplet state energy level of the ligand and lanthanide(III) luminescence quantum yield. J Lumin. 75 (1997), p.p.149-69.

[4] C. Bizzarri, Spuling E., Knoll D. M., Volz D., Bräse S. Sustainable metal complexes for organic light-emitting diodes (OLEDs). Coord Chem Rev. 373 (2018), p.p.49-82.

[5] L. F. Pereira. Organic light emitting diodes: The use of rare earth and transition metals: CRC Press, 2012.

[6] L. F. Marques, Cuin A., de Carvalho G. S. G., dos Santos M. V., Ribeiro S. J. L., Machado F. C. Energy transfer process in highly photoluminescent binuclear hydrocinnamate of europium, terbium and gadolinium containing 1,10-phenanthroline as ancillary ligand. Inorg Chim Acta. 441 (2016), p.p.67-77.

[7] (a) M. Starck, Fradgley J. D., Pal R., Zwier J. M., Lamarque L., Parker D. Synthesis and Evaluation of Europium Complexes that Switch on Luminescence in Lysosomes

of Living Cells. Chem Eur J. 27 (2021), p.p.766-77; (b) L. Abad-Galán, Cieslik P., Comba P., Gast M., Maury O., Neupert L., Roux A., Wadepohl H. Excited State Properties of Lanthanide(III) Complexes with a Nonadentate Bispidine Ligand. Chem Eur J. 27 (2021), p.p.10303-12; (c) B. Golesorkhi, Nozary H., Fürstenberg A., Piguet C. Erbium complexes as pioneers for implementing linear light-upconversion in molecules. Materials Horizons. 7 (2020), p.p.1279-96; (d) J. H. S. K. Monteiro, Hiti E. A., Hardy E. E., Wilkinson G. R., Gorden J. D., Gorden A. E. V., de Bettencourt-Dias A. New up-conversion luminescence in molecular cyano-substituted naphthylsalophen lanthanide(iii) complexes. Chem Commun. 57 (2021), p.p.2551-4.

[8] L. Wang, Zhao Z., Wei C., Wei H., Liu Z., Bian Z., Huang C. Review on the Electroluminescence Study of Lanthanide Complexes. Adv Opt Mater. 0 (2019), p.p.1801256.

[9] A. Døssing. Luminescence from Lanthanide(3+) Ions in Solution. Eur J Inorg Chem. 2005 (2005), p.p.1425-34.

[10] (a) K. Binnemans. Rare-earth beta-diketonates. In: K.A. Gschneidner JCB, Pecharsky VK, editors. Handbook on the Physics and Chemistry of Rare Earths: Elsevier; 2005. p. 107-272; (b) K. Binnemans. Interpretation of europium(III) spectra. Coord Chem Rev. 295 (2015), p.p.1-45; (c) C. D. S. Brites, Millán A., Carlos L. D. Chapter 281 - Lanthanides in Luminescent Thermometry. In: Jean-Claude B, Vitalij K P, editors. Handbook on the Physics and Chemistry of Rare Earths: Elsevier; 2016. p. 339-427; (d) J.-C. G. Bünzli. Chapter 287 - Lanthanide Luminescence: From a Mystery to Rationalization, Understanding, and Applications. In: Bünzli J-CG, Pecharsky VK, editors. Handbook on the Physics and Chemistry of Rare Earths: Elsevier; 2016. p. 141-76; (e) R. Ilmi, Khan M. S., Sun W., Zhou L., Wong W.-Y., Raithby P. R. A single component white electroluminescent device fabricated from a metallo-organic terbium complex. J Mater Chem C. 7 (2019), p.p.13966-75; (f) R. Ilmi, Anjum S., Haque A., Khan M. S. A new brilliant red emitting Eu(III) ternary complex and its transparent flexible and photostable poly(urethane) hybrid thin film for optoelectronic applications. J Photochem Photobiol, A. 383 (2019), p.p.111968; (g) J. Sun, Song B., Ye Z., Yuan J. Mitochondria Targetable Time-Gated Luminescence Probe for Singlet Oxygen Based on a β-Diketonate-Europium Complex. Inorg Chem. 54 (2015), p.p.11660-8.

[11] (a) D. Kovacs, Borbas K. E. The role of photoinduced electron transfer in the quenching of sensitized Europium emission. Coord Chem Rev. 364 (2018), p.p.1-9; (b) R. Ilmi, Kansız S., Dege N., Khan M. S. Synthesis, structure, Hirshfeld surface analysis and photophysical studies of red emitting europium acetylacetonate complex incorporating a phenanthroline derivative. J Photochem Photobiol, A. 377 (2019), p.p.268-81.

[12] Z. Bian. Electroluminescent properties of three ternary europium complexes with different phenanthroline derivatives. Sci China Ser B. 47 (2004), p.p.326.

[13] (a) I. J. Al-Busaidi, Ilmi R., Dutra J. D. L., Oliveira W. F., Haque A., Al Rasbi N. K., Marken F., Raithby P. R., Khan M. S. Utilization of a Pt(ii) di-yne chromophore incorporating a 2,2'-bipyridine-5,5'-diyl spacer as a chelate to synthesize a green and red emitting d-f-d heterotrinuclear complex. Dalton Trans. 50 (2021), p.p.1465-77; (b) R. Ilmi, Haque A., Al-Busaidi I. J., Al Rasbi N. K., Khan M. S. Synthesis and photophysical properties of hetero trinuclear complexes of tris β-diketonate Europium with organoplatinum chromophore. Dyes Pigm. 162 (2019), p.p.59-66.

[14] (a) H. J. Batista, de Andrade A. V. M., Longo R. L., Simas A. M., de Sá G. F., Thompson L. C. Synthesis, crystal structure determination and theoretical prediction of the structure and electronic spectrum of Eu(btfa)3bipy. J Lumin. 72-74 (1997), p.p.159-61; (b) H. J. Batista, de Andrade A. V. M., Longo R. L., Simas A. M., de Sá G. F., Ito N. K., Thompson L. C. Synthesis, X-ray Structure, Spectroscopic Characterization, and Theoretical Prediction of the Structure and Electronic Spectrum of Eu(btfa)3·bipy and an Assessment of the Effect of Fluorine as a β-Diketone Substituent on the Ligand−Metal Energy Transfer Process. Inorg Chem. 37 (1998), p.p.3542-7.

[15] M. S. Khan, Ilmi R., Sun W., Dutra J. D. L., Oliveira W. F., Zhou L., Wong W.-Y., Raithby P. R. Bright and efficient red emitting electroluminescent devices fabricated from ternary europium complexes. J Mater Chem C. 8 (2020), p.p.5600-12.

[16] D. F. Eaton. International Union of Pure and Applied Chemistry Organic Chemistry Division Commission on Photochemistry. Reference materials for fluorescence measurement. J Photochem Photobiol B. 2 (1988), p.p.523-31.

[17] N. B. D. Lima, Gonçalves S. M. C., Júnior S. A., Simas A. M. A Comprehensive Strategy to Boost the Quantum Yield of Luminescence of Europium Complexes. Sci Rep. 3 (2013), p.p.2395.

[18] M. H. V. Werts, Jukes R. T. F., Verhoeven J. W. The emission spectrum and the radiative lifetime of Eu3+ in luminescent lanthanide complexes. Phys Chem Chem Phys. 4 (2002), p.p.1542-8.

[19] R. Ilmi, Hasan N., Liu J., Mara D., Van Deun R., Iftikhar K. Effect of 2,4,6-tri(2-pyridyl)-1,3,5-triazine on visible and NIR luminescence of lanthanide tris(trifluoroacetylacetonates). J Photochem Photobiol, A. 347 (2017), p.p.116-29.

[20] S. Sato, Wada M. Relations between Intramolecular Energy Transfer Efficiencies and Triplet State Energies in Rare Earth β-diketone Chelates. Bull Chem Soc Jpn. 43 (1970), p.p.1955-62.

[21] W. T. Carnall, Crosswhite H., Crosswhite H. M. Energy level structure and transition probabilities in the spectra of the trivalent lanthanides in LaF3. . 1978. p. Pages: 185.

[22] R. Ilmi, Iftikhar K. Optical emission studies of new europium and terbium dinuclear complexes with trifluoroacetylacetone and bridging bipyrimidine. Fast radiation and high emission quantum yield. Polyhedron. 102 (2015), p.p.16-26.

[23] R. Ilmi, Haque A., Khan M. S. Synthesis and photo-physics of red emitting europium complexes: An estimation of the role of ancillary ligand by chemical partition of radiative decay rate. J Photochem Photobiol, A. 370 (2019), p.p.135-44.

[24] E. Kasprzycka, Carneiro Neto A. N., Trush V. A., Jerzykiewicz L., Amirkhanov V. M., Malta O. L., Legendziewicz J., Gawryszewska P. How minor structural changes generate major consequences in photophysical properties of RE coordination compounds; resonance effect, LMCT state. J Rare Earths. 38 (2020), p.p.552-63.

[25] (a) P.-P. Sun, Duan J.-P., Shih H.-T., Cheng C.-H. Europium complex as a highly efficient red emitter in electroluminescent devices. Appl Phys Lett. 81 (2002), p.p.792-4; (b) F. Liang, Zhou Q., Cheng Y., Wang L., Ma D., Jing X., Wang F. Oxadiazole-Functionalized Europium(III) β-Diketonate Complex for Efficient Red Electroluminescence. Chem Mater. 15 (2003), p.p.1935-7.

[26] C. Adachi, Baldo M. A., Forrest S. R. Electroluminescence mechanisms in organic light emitting devices employing a europium chelate doped in a wide energy gap bipolar conducting host. J Appl Phys. 87 (2000), p.p.8049-55.

[27] J. Kido, Hayase H., Hongawa K., Nagai K., Okuyama K. Bright red light‐emitting organic electroluminescent devices having a europium complex as an emitter. Appl Phys Lett. 65 (1994), p.p.2124-6.

[28] H. Xu, Wang L.-H., Zhu X.-H., Yin K., Zhong G.-Y., Hou X.-Y., Huang W. Application of Chelate Phosphine Oxide Ligand in EuIII Complex with Mezzo Triplet Energy Level, Highly Efficient Photoluminescent, and Electroluminescent Performances. J Phys Chem B. 110 (2006), p.p.3023-9.